CHALMERS
UNIVERSITY OF TECHNOLOGY

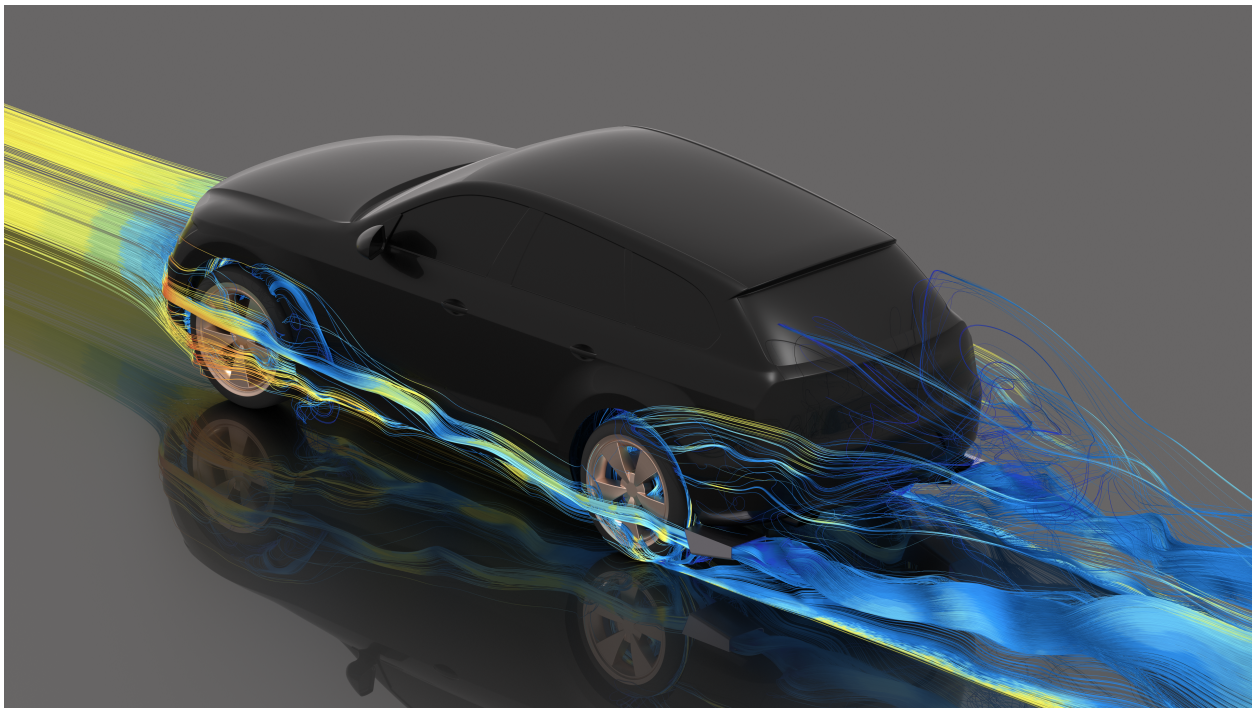

# Numerical investigations of the flow around rotating wheels with the purpose of tracing tyre dust

TARUN KADRI SATHIYAN

DEPARTMENT OF MECHANICS AND MARITIME SCIENCES
CHALMERS UNIVERSITY OF TECHNOLOGY
Gothenburg, Sweden 2022
www.chalmers.se

MASTER'S THESIS IN AUTOMOTIVE ENGINEERING

# Numerical investigations of the flow around rotating wheels with the purpose of tracing tyre dust

TARUN KADRI SATHIYAN

Department of Mechanics and Maritime Sciences
*Division of Vehicle Engineering and Autonomous Systems*
CHALMERS UNIVERSITY OF TECHNOLOGY
Gothenburg, Sweden 2022

Numerical investigations of the flow around rotating wheels with the purpose of tracing tyre dust
TARUN KADRI SATHIYAN



Supervisor: Thomas Hult, (CEVT) China Euro Vehicle Technology AB
Supervisor: Andrew Dawkes, (CEVT) China Euro Vehicle Technology AB
Examiner: Alexey Vdovin, Department of Mechanics and Maritime Sciences

Master's Thesis 2022:34
Department of Mechanics and Maritime Sciences
Division of Vehicle Engineering and Autonomous Systems
Chalmers University of Technology
SE-412 96 Gothenburg
Telephone +46 31 772 1000

Cover: The AeroSUV vehicle depicting streamlines originating at the tyre patch and through TTC's device mounted behind the rear wheels.

Chalmers Digitaltryck
Gothenburg, Sweden 2022

Numerical investigations of the flow around rotating wheels with the purpose of tracing tyre dust

TARUN KADRI SATHIYAN
Department of Mechanics and Maritime Sciences
Division of Vehicle Engineering and Autonomous Systems
Chalmers University of Technology

# Abstract

As we move into an era of electrification of vehicles, there is a constant need to suppress the environmental impact caused by these vehicles. Electric vehicles have drastically lowered exhaust gas emissions but on the flip-side, it has significantly increased non-exhaust emissions. With more than 1 billion passenger vehicles roaming the streets today, it is evident that non-exhaust emissions will only rise in the upcoming years as more BEVs are churned out by manufacturers.

Non-exhaust emissions majorly constitutes of tyre wear and brake wear. Several experiments have shown the particulate matter that is abraded off the tyres is charged and hence can be trapped using static electricity. In this work, the complex flow around rotating wheels and inside the wheelhouse is investigated. The work also extends into investigating the effectiveness of a device obtained from The Tyre Collective, which captures these particulate emissions. Using numerical simulations, a generic model of the AeroSUV is studied along with TTC's device. It was determined that the device placement is not ideal and, having an externally mounted device is prone to vibrations and contamination due to soiling.

The change in overall drag and rear wake profile is shown with the help of a comparison study of the vehicle with and without the device. The shape of the device has been shown to restrict flow behind the rear wheels to some extent. Additionally, flow recirculation at the inlet of the device is shown using streamline tracers. The study also shows that the majority of the mass flow of air through the device comes from the front, through the underbody. Furthermore, based on the numerical analysis several design recommendations were provided.

Lastly, this investigative study has shown that simulating particles using multiphase will be worthwhile in providing more information and, a numerical method for both wheel rotation modelling and particle tracing. Furthermore, upcoming Euro 7 emission norms are speculated to have stringent regulations on tyre and brake wear. Hence, capturing these particulate emissions at the source would be highly beneficial and to do so, a more sophisticated numerical analysis of particle behaviour is necessary to decipher the optimal methods to capture them.

Keywords: Vehicle aerodynamics, CFD, AeroSUV, wheel rotation, tyres, tyre dust, zero emissions, non-exhaust emissions.

# Acknowledgements

I would like to thank my examiner and supervisor at Chalmers, Dr. Alexey Vdovin, for all his support and guidance throughout this thesis work. His inputs greatly contributed to the outcome of this project and improved the quality of work. From giving me support with everyday issues to productive discussions, I cannot thank him enough for providing me with instantaneous feedback and making it less stressful for me.

The project was conducted in collaboration with CEVT. I would like to express my gratitude to both my industrial supervisors, Thomas Hult and Andrew Dawkes, for always being supportive and connecting me with the right people to get work done. Special thanks to my manager, Per-Erik Kronqvist, for getting me in touch with The Tyre Collective and, for his consistent support and interest in this project.

Thank you to everyone at The Tyre Collective, for providing me with all of the information and the brainstorming sessions. Special thanks to Siobhan Anderson and Hugo Richardson for always keeping me in the loop.

Thanks to all my friends and colleagues. I would like to express my gratitude to Ph.D. students at VEAS for helping me out with some of my numerical setups and for sharing their thoughts. Special thanks to Dr. Simone Sebben, head of the division, for creating an amazing and flexible work atmosphere. Thanks to Sonja Laakso Gustafsson for keeping me updated with all additional information and documents related to my thesis work.

Finally, I would like to thank my parents and grandparents, for their constant support and encouragement to pursue my goals. Thanks to my little brother for always looking out for me.

Tarun Kadri Sathiyan
Gothenburg, June 2022

# Nomenclature

## Symbols

| | |
|---|---|
| $C_d$ | Aerodynamic drag coefficient |
| $C_p$ | Pressure coefficient |
| $C_{ptot}$ | Total pressure coefficient |
| $C_{lf}$ | Lift coefficient on front axle |
| $C_{lr}$ | Lift coefficient on rear axle |

## Abbreviations

| | |
|---|---|
| BEV | Battery Electric Vehicles |
| CAD | Computer-aided Design |
| CFD | Computational Fluid Dynamics |
| IDDES | Improved Delayed Detached-Eddy Simulation |
| MRF | Moving Reference Frame |
| PM | Particulate Matter |
| RANS | Reynolds Averaged Navier Stokes |
| URANS | Unsteady or Transient Reynolds Averaged Navier Stokes |
| TWP | Tyre Wear Particles |

# Contents

# List of Figures

# 1

# Introduction

Road transport plays a substantial role in the modern world. To be specific, passenger vehicles cover a considerable segment of all road transportation. It is of peak interest to mitigate the negative effects of these vehicles. Exhaust gases or tail-pipe emission is one such effect that has been a reason to switch to electric or hybrid vehicles. Electrified transportation systems allow for a more energy-efficient and environmentally friendly alternative to traditional vehicles equipped with internal combustion engines [1]. Over the past decade, this change has drastically lowered the amount of tail-pipe emissions. Moreover, stringent regulations on exhaust gases have largely helped lower tail-pipe particulate emissions. On the other hand, electrified vehicles bring new challenges: To a great degree, the rise of non-exhaust emissions from road vehicles [2].

Non-exhaust emissions are categorised into - tyre dust, brake dust, and road dust resuspension. Tyre wear particles (TWP) and brake wear particles (BWP) are deemed to be major contributors to non-exhaust emissions. This study is directed toward TWPs. Due to complex flow patterns around rotating wheels and the chaotic flow inside the wheelhouse, it is essential to study the flow patterns to effectively capture TWPs.

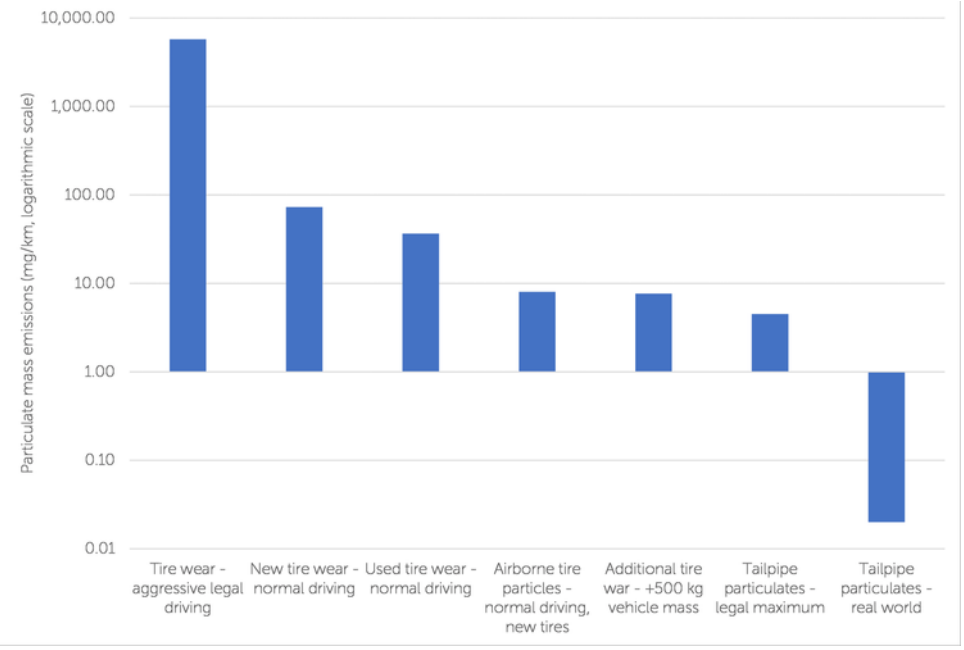


**Figure 1.1:** Tyre wear particulate mass emissions in mg/km for various scenarios [8]

Research has shown that the emitted PM from tyres majorly is within the range of PM2.5 and PM10 which is representative of particle sizes of $2.5\mu m$ and $10\mu m$ respectively. But there are particles less than $1\mu m$ [3]. All these particles are generally airborne and hence follow the flow stream for the most part. A study conducted in Norway estimated that there is 19000 t/year of microplastics released from terrestrial sources. However, tyre wear and road dust contribute to about 40% of it [7]. Studies have shown that a considerable proportion of tyre wear particulate emissions are in smaller fractions (less than PM10) especially in roads with heavy traffic [5]. Figure 1.1 shows tyre wear particulate mass emissions in mg/km for various scenarios. The study showed that 11% by mass of emissions from tyre wear are smaller than PM2.5. The legal limitation for tailpipe emissions is 4.5 mg/km whereas experimental data for airborne tyre emissions shows that it is around 8 mg/km [8].

## 1.1 Project objectives

This master thesis project is conducted at Chalmers University of Technology in collaboration with CEVT. The main objective of this work is to study the airflow around rotating wheels using CFD simulations to determine effective ways of capturing tyre dust. The objectives of this project are as follows:

- Identify the factors affecting TWPs based on an elaborate literature review.
- Determine and setup an effective numerical simulation methodology for wheel rotation and the flow around wheels for investigating the AeroSUV geometry along with TTC's device (This research study is vehicle specific and dependent on the orientation of the device).
- Simulate the particles originating at the tyre patch that follows the airflow.
- Propose design strategies to efficiently capture TWPs.

## 1.2 Limitations

- The project is mainly limited in terms of computational resources, impeding the mesh quality and the physics models implemented.
- Given the time constraint to complete the entire project, only a few physics models are implemented in this study.
- The investigations were only performed using a simplified SUV model in the estateback configuration.
- Only one configuration of TTC's device with a simplified geometry representing the outer shell is considered throughout this study.

# 2
# Background

This chapter gives an elaborate literature study motivating the reason behind this thesis work. Furthermore, the background on effectively modelling wheel rotation which allows for a better understanding of the flow.

## 2.1 Non-exhaust emissions and its environmental impact

In general, emissions of PM from road transportation consist of two sources namely - exhaust gases from internal combustion engines and emissions caused due to degradation of vehicle parts due to friction. Tyre wear, brake wear, and road dust are classified as non-exhaust emissions and the magnitude of these non-exhaust emissions has drastically risen over the past years. It is now responsible for approximately 90% of all PM emissions from road transportation [17, 18].

Non-exhaust PM emissions are classified as follows [2]:

- Direct wear emissions:
  - Tyre wear - airborne particles abraded from tyres.
  - Brake wear - eroded particles from brake disc and pads. Only 50% of the emitted brake dust is considered to be airborne.
  - Road wear - airborne particles eroded from the surface of tarmac.
- Road dust resuspension - suspended particles on road surfaces caused due to road transport

Governmental regulations and public awareness of the negative effects of transportation on the environment have led to the electrification of vehicles to counteract some of the major drawbacks caused by internal combustion engines, such as tailpipe emissions. While legislation has driven down emissions of particles from exhaust gases, the non-exhaust proportion of road traffic emissions has been increasing drastically over the past decade [2]. BEVs are typically heavier relative to traditional vehicles with internal combustion engines because of the additional battery mass. Hence, BEVs requires wider and larger tyres which has a larger tyre patch. According to Emissions Analytics, particulate emissions from tailpipes are much lower on newer vehicles whereas tyre wear particulate emissions increase with aggressive driving style and vehicle mass[8]. Figure 2.1 shows the projected PM2.5 emissions from tyre and road surface wear relative to tailpipe emissions [10] obtained from a recent study in the United Kingdom.

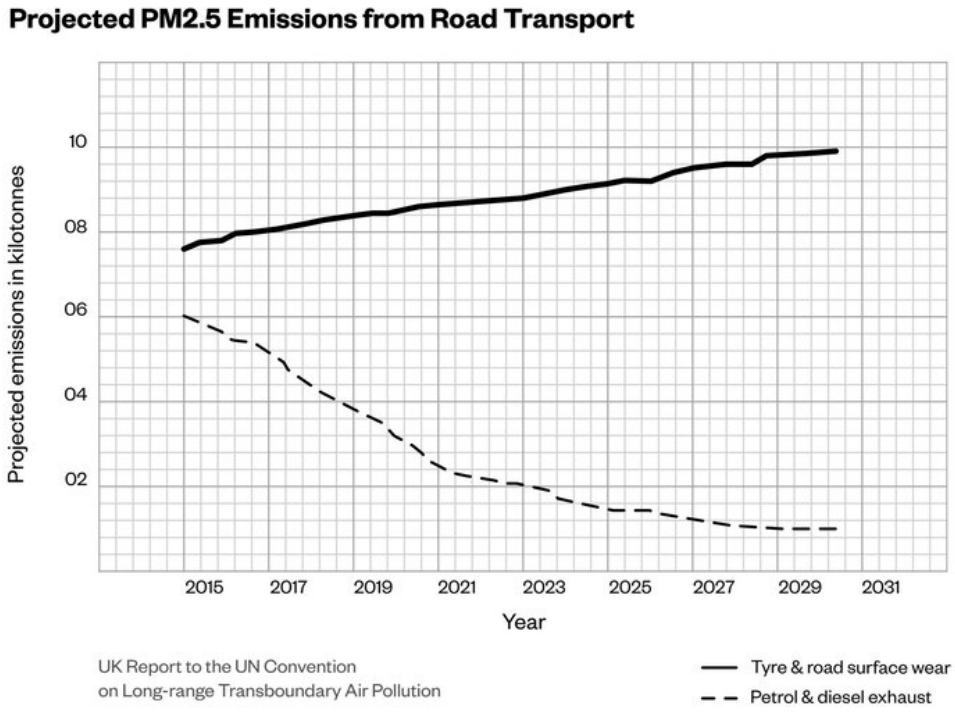


**Figure 2.1:** Projected particulate matter emissions from road transport [10]

On a global scale, human exposure to these air-borne PMs is hazardous and can cause a significant impact on human health. Especially, considering that these PMs are small enough in micro scales to enter our respiratory system. This can be carcinogenic when humans are exposed to these PMs over a long period. Moreover, it can cause multiple lung-related issues such as asthma, blockage in a lung artery, etc. Hence, lowering air pollution in an urban environment is crucial to reducing ambient toxicity levels and maintaining good air quality [16].

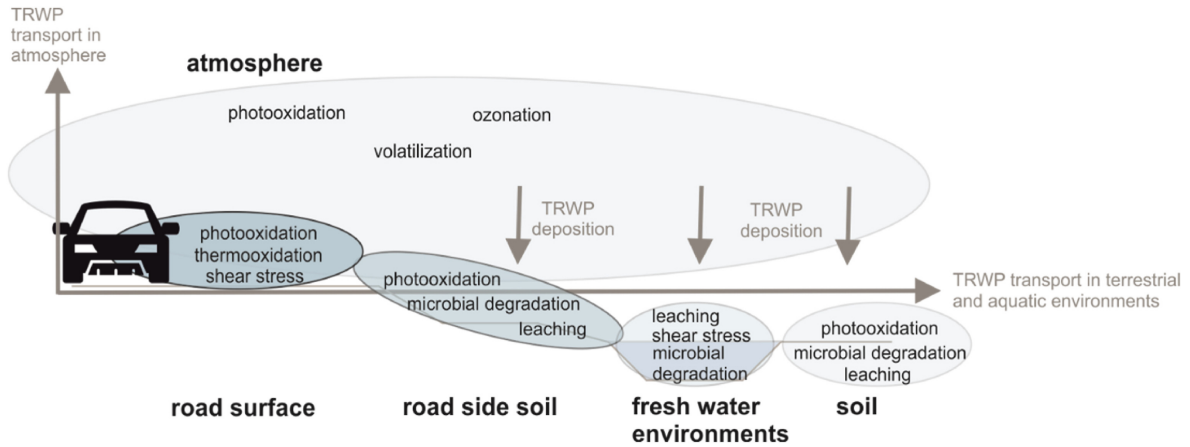


**Figure 2.2:** Tyre and road wear particles (TRWP) aging processes on road surface, in the atmosphere, soil and water bodies [6]

A significant amount of PM from tyre wear ends up in water bodies contaminating the aquatic body and aquatic soil. This has a significant impact on aquatic life, damaging the natural habitat. Figure 2.2 shows the aging processes of tyre and road wear particles on road surface, atmosphere, soil and water [6]. There are not a lot of studies involved in investigating the ageing process of tyre and road particles in water bodies. However, data indicates that there is a rise in microplastics in aquatic bodies.

## 2.2 Literature review

### 2.2.1 Tyre dust

Although there is insubstantial contemplation on the characterization of TWPs, various research groups have invested time in determining the toxicity levels of tyre wear debris in our environment. TWPs have been implicated to be very toxic to humans through aquatic bodies based on the potential to induce endocrine disruption, acute lethality, and teratogenicity. Moreover, research has also proven that the airborne magnitude of TWPs can induce in-vitro or in-vivo pulmonary poisoning [24] if inhaled by humans.

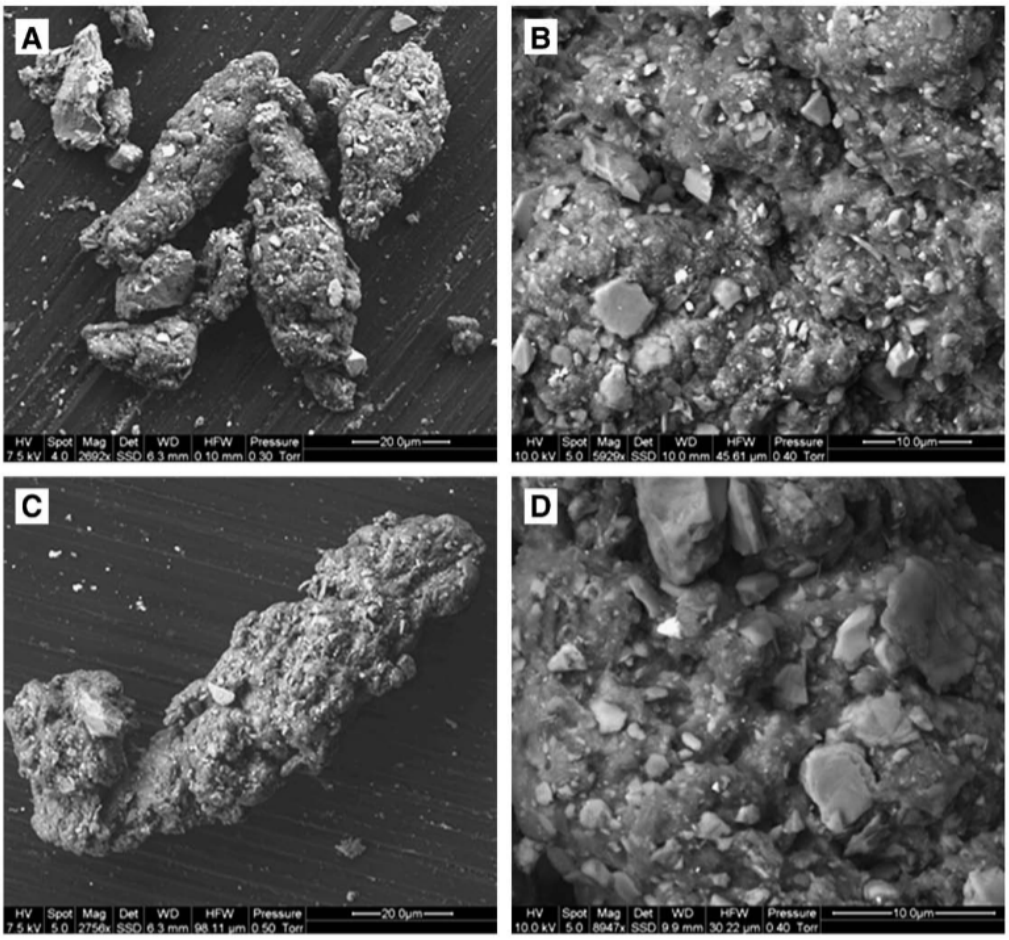


**Figure 2.3:** Microscopic images of road particles and TWPs [21]

Tyre dust or tyre wear is the result of tyre tread abrasion on the surface of tarmac. Scanning electron microscope (SEM) images have shown these particles to have an elongated or "sausage-like" shape. Chemical analysis of these particles shows that they include rubber from the tyres, as well as encrusted mineral particles from road surfaces [19, 21]. Figure 2.3 indicates the SEM images of road particles (A,B) and TWPs (C,D). It shows that TWPs consist of a higher mineral content [21].

Since airborne TWPs are relatively smaller in size, physical properties also play a major role in their chemical composition. This includes the temperature of the tyres, ambient temperature, roughness of the road surface, etc.

### 2.2.2 Particle size distribution

#### 2.2.2.1 Tyre wear particles

Studies that have been conducted in the past have shown that tyre dust particle sizes vary with the type of tyre i.e., studded or non-studded and also the type of tarmac [25]. The table shown in Figure 2.5 depicts the amount of PM10 emitted in mg/km. 50% to 70% of all airborne road dust falls under the category of PM10.


**Figure 2.4:** Emitted particles from various means of transportation [10]

Figure 2.4 illustrates the amount of tyre wear collected from various sources of road transport in one day. Approximately, 1 to 2kg of total tyre wear on passenger vehicles is estimated over a typical life-cycle of about 70000km [23]. Studies have also shown that since BEVs require wider tyres as they are heavier, the larger contact patch creates more traction with the road surface. Thus, generating more TWPs. Lab tests have also shown that the size distribution of TWPs varies significantly [11], concerning various driving factors including tangential wheel velocity, ambient temperature, load on the

tyres, acceleration, harsh braking, and lateral slip. The emitted TWP hence has a range of varied sizes, both "traditional" particles (2.5 - 10$\mu m$) but also smaller particles (<1$\mu m$), depending on the conditions [3].

#### 2.2.2.2 Brake wear particles

Brake wear particles mostly fall within the size range of 2$\mu m$ to 5$\mu m$. Recent studies have also shown an increase in nano-sized brake wear caused due to extreme temperature conditions [9]. This speculation can also be carried forth on TWPs as they exhibit similarities in particle sizes and behavioural change with respect to temperature effects. Emissions from brake wear is considered as the most metal-rich airborne particulate emission from road transport. Out of all the chemical constituents of brake dust, iron in its ferrous form ($Fe^{2+}$) is deemed to play a role in human cardiovascular and neurological defacement [15].

| mg $PM_{10}$ / km | | Tyre | Brake |
|---|---|---|---|
| Cars | Urban | 8.7 | 11.7 |
| | Rural | 6.8 | 5.5 |
| | Motorway | 5.8 | 1.4 |
| LGVs | Urban | 13.8 | 18.2 |
| | Rural | 10.7 | 8.6 |
| | Motorway | 9.2 | 2.1 |
| Rigid HGVs | Urban | 20.7 | 51.0 |
| | Rural | 17.4 | 27.1 |
| | Motorway | 14.0 | 8.4 |
| Artic HGVs | Urban | 47.1 | 51.0 |
| | Rural | 38.2 | 27.1 |
| | Motorway | 31.5 | 8.4 |
| Buses | Urban | 21.2 | 53.6 |
| | Rural | 17.4 | 27.1 |
| | Motorway | 14.0 | 8.4 |
| Motorcycles | Urban | 3.7 | 5.8 |
| | Rural | 2.9 | 2.8 |
| | Motorway | 2.5 | 0.7 |

**Figure 2.5:** Emission factors for PM10 from tyre and brake wear [22]

### 2.2.3 TTC's device

The Tyre Collective is a startup based in the UK who are investigating methods of capturing tyre particles at the source of emission. An experimental study on tyre particles showed that the particles are charged because of the friction between the tyres and road surface. The illustration shown in Figure 2.6 indicates a concept where the device is mounted very close to the tyres. The device consists of an array of electrostatic plates that can be charged or discharged using the battery on the vehicle. The electrostatic field that is generated, attracts the tyre dust which adheres to these plates as shown in Figure 2.7 which is from an experimental study that The Tyre Collective had conducted [10].

**Figure 2.6:** Conceptual design of TTC's device [10]

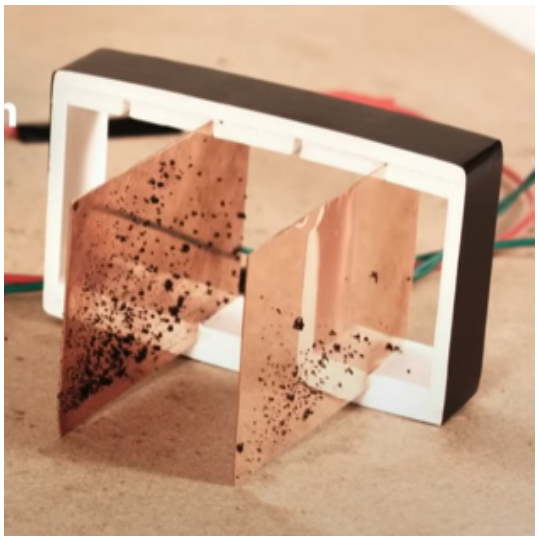

**Figure 2.7:** Electrostatic plates with tyre wear adhered to it [10]


**Figure 2.8:** Device used for capturing PM [4]

Figure 2.8 shows a physical prototype of the device from The Tyre Collective that was mounted onto a vehicle and tested in Gothenburg. The experiment was carried out in collaboration with CEVT and The Tyre Collective.

# 3
# Methodology

## 3.1 Vehicle geometry

Figure 3.1 shows the dimensions of the full-scale AeroSUV from the European Car Aerodynamics Research Association (ECARA) [13, 14] in the baseline variant which is the exact configuration utilised in this thesis work with open grilles. This is a generic SUV model that is used in aerodynamics research. The estate-back variant of the AeroSUV is used throughout this study as it represents a larger and heavier passenger vehicle. Also, the experimental tests conducted by The Tyre Collective is on an SUV. The model has open cooling or air intakes at the front and a relatively detailed underbody.

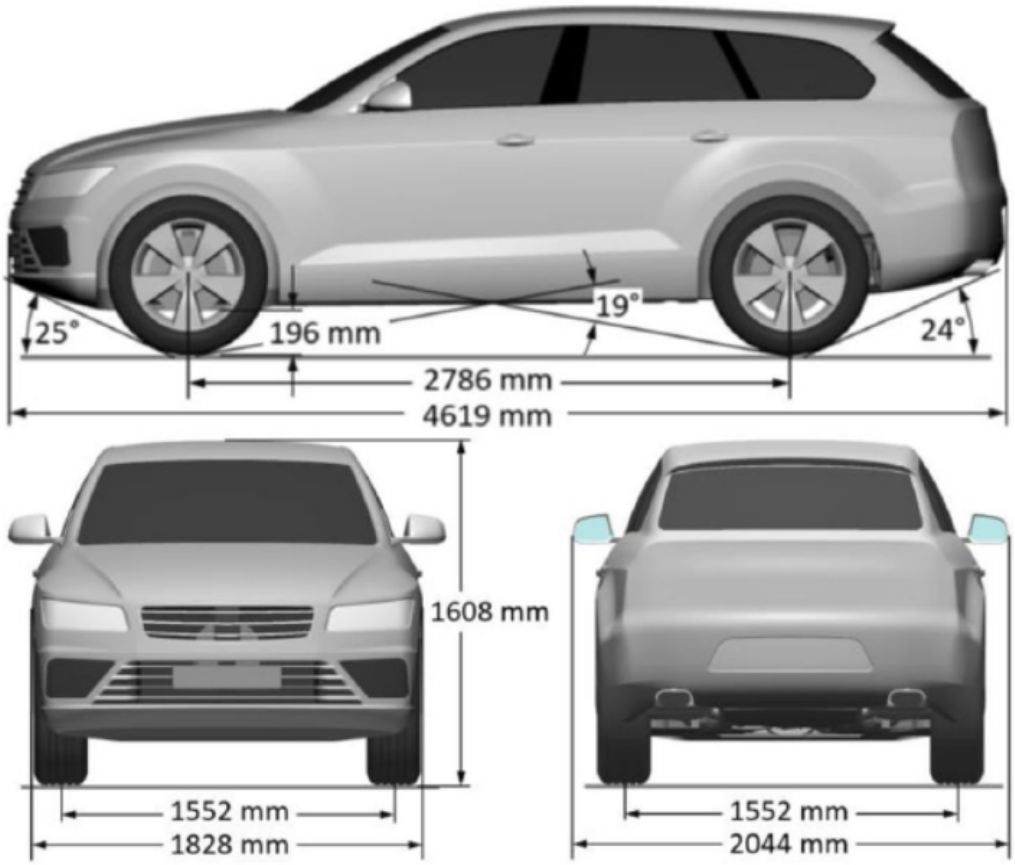


**Figure 3.1:** Dimensions of the baseline full-scale AeroSUV [14]

The AeroSUV is characterised with a larger cross-sectional area, increased ground clear-

ance and larger wheels in comparison to the standard DrivAer model. The AeroSUV represents a mid-class SUV derived from the DrivAer [14]. This particular model contains a level of detail which is comparable to today's production cars by inclusion of a detailed underbody and engine bay to allow under-hood cooling flow. The AeroSUV can represent a vehicle with an engine or a BEV in estate, notch or fast-back configurations [13]. Figure 3.2 depicts the vehicle geometry of the AeroSUV . Additionally, a simplified TTC's device consisting of the outer shell of the prototype as shown below in Figure 3.3 is included with the vehicle, mounted behind the rear wheels.

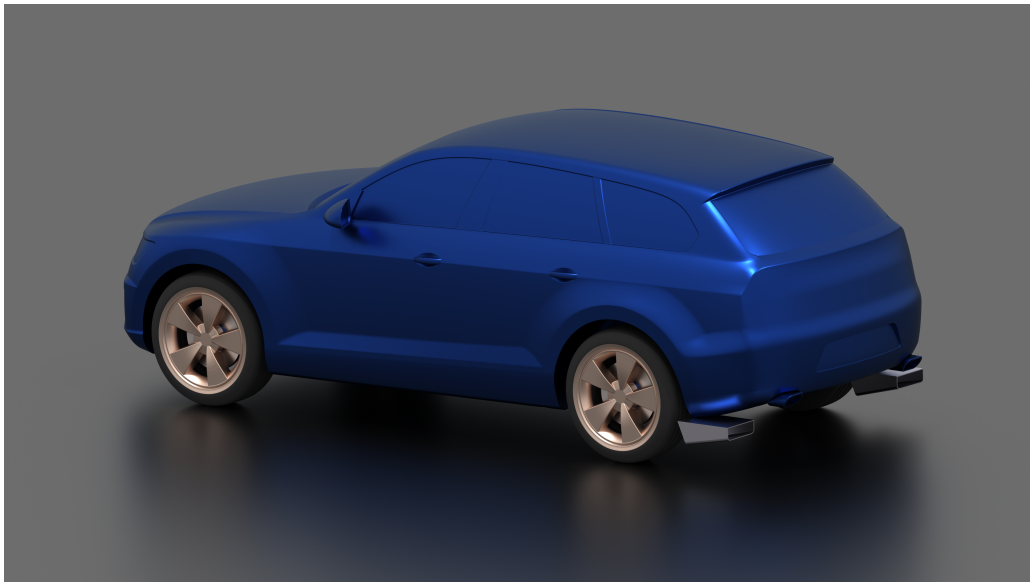

**Figure 3.2:** AeroSUV model

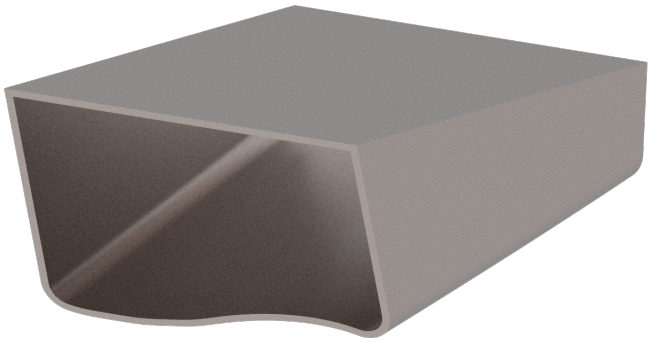

**Figure 3.3:** Simplified geometry of TTC's device

## 3.2 Numerical setup

Pre-processing of CAD for both the vehicle geometry and TTC's device was carried out using ANSA software. Figure 3.2 shows the resultant of the imported geometry for further numerical simulations. However, there were additional surfaces added to the original geometry to isolate areas of different mesh types such as a sliding mesh region for rims. All of the numerical computations were performed using a commercial CFD software - Star-CCM+. This section discusses the computational domain, different meshing strategies, and various implemented physics models.

### 3.2.1 Computational domain

To replicate an open road, an elongated rectangular computational domain is implemented as shown in Figure 3.4 measuring 100m in length, 30m in width, and 20m in height. The dimensions of the domain are made large enough to avoid unnecessary formations of boundary layers and to avoid blockage effects that may influence the obtained results.

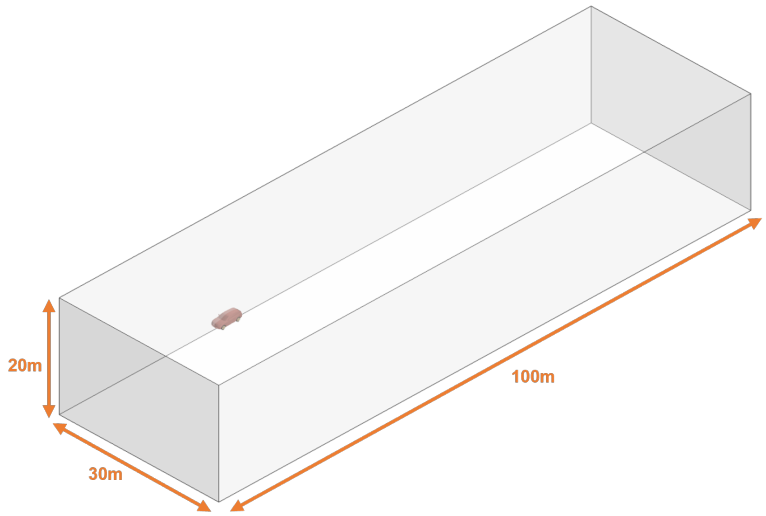


**Figure 3.4:** Open road domain used in numerical simulations

The vehicle is placed approximately 30 m from the inlet and in such a way that only half the vehicle geometry is inside the domain as shown in Figure 3.7. This is done mainly due to the constraints on computational resources and the requirement of a finer mesh close to the wheels. An assumption that is made with regard to the previously mentioned factors is that the vehicle is longitudinally symmetrical. Hence, a symmetry plane through the vehicle. The open road domain consisted of a constant inlet velocity of 10 m/s and pressure outlet boundary condition of 0 Pa. The inlet velocity of 10m/s lies in-between a velocity range at which tyre wear emissions are estimated to be high. The inlet velocity specification is also used to determine the velocity of the moving ground and the tangential velocity of wheels. The boundary condition for the road is assigned as a moving wall. The rest of the walls were assigned with a no-slip wall boundary condition.

### 3.2.2 Wheel rotation modelling and tyre aerodynamics

Figure 3.5 shows the general wheel terminology used throughout this thesis work.

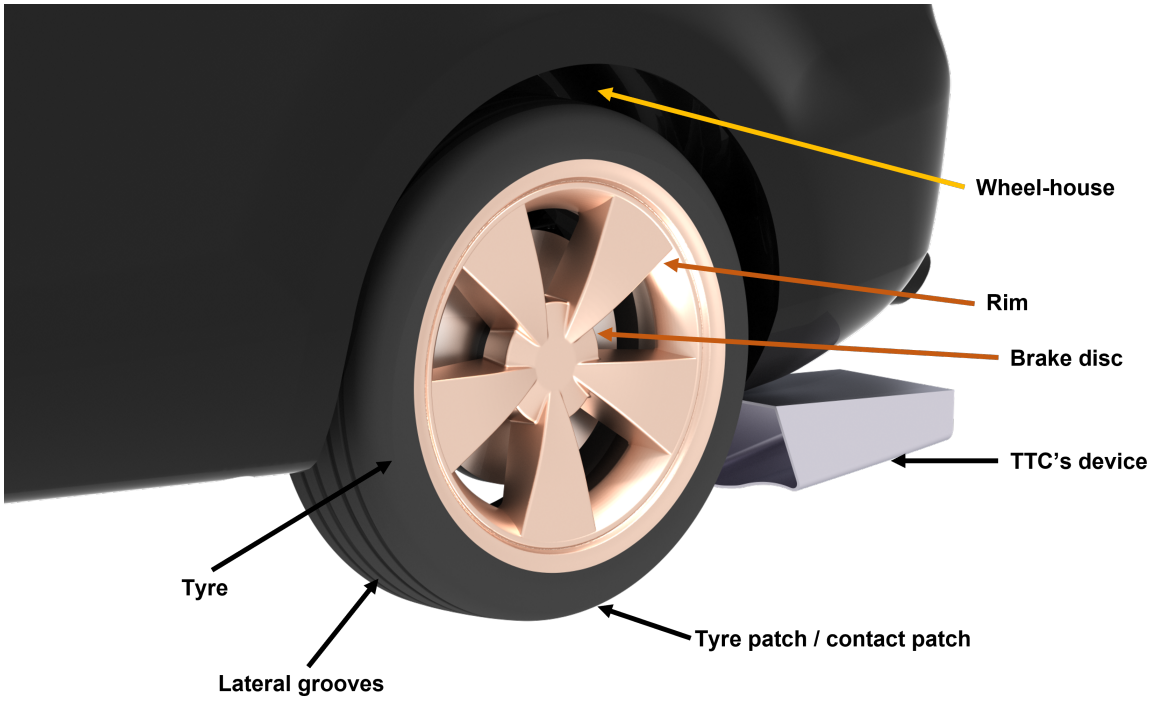


**Figure 3.5:** Nomenclature used for various features on the wheels

Wheel rotational modelling brings its own challenges and modelling wheel rotation to get as close as possible to reality is key in studying the highly turbulent flow around the wheels and in the wheelhouse. Traditionally, there exist three approaches to simulating wheel rotation, namely - moving wall, MRF (Moving Reference Frame), and Sliding mesh. Firstly, a moving wall approach is executed by applying a rotational velocity on the moving boundary. This method is not recommended when the desired velocity is normal to cell surface as in rims because this method only applies a velocity tangential to the wall. Secondly, an MRF approach allows for a surface velocity normal to the surface. This can produce the desired velocity only if the entire wheel is inside the MRF region. Lastly, a sliding mesh approach is executed by physical rotation of the mesh at every specified time-step. This modelling method is the closest to reality. [20]

Various studies that focus on modelling wheel rotation have shown that physical wheel rotation or having a sliding mesh result in separation at the top of the tyre relative to a stationary wheel [12]. In this case, since the focus is to study the movement of PM with respect to airflow, it is more suitable to have a sliding mesh to include the additional effects of physically rotating the mesh which significantly varies the flow behaviour.

Figure 3.6 represents a cross-sectional view of a single wheel showcasing the sliding mesh region for the rim and its interfaces. The interfacing is implemented such that the cells inside the sliding mesh region close to the interfaces communicate with the cells outside the region. For this study, the rims in magenta as shown in Figure 3.7 are the sliding

mesh regions, and the tyres indicated in blue is assigned with a rotating wall boundary condition. Both MRF and sliding mesh approaches were compared to study the differences in flow structures.

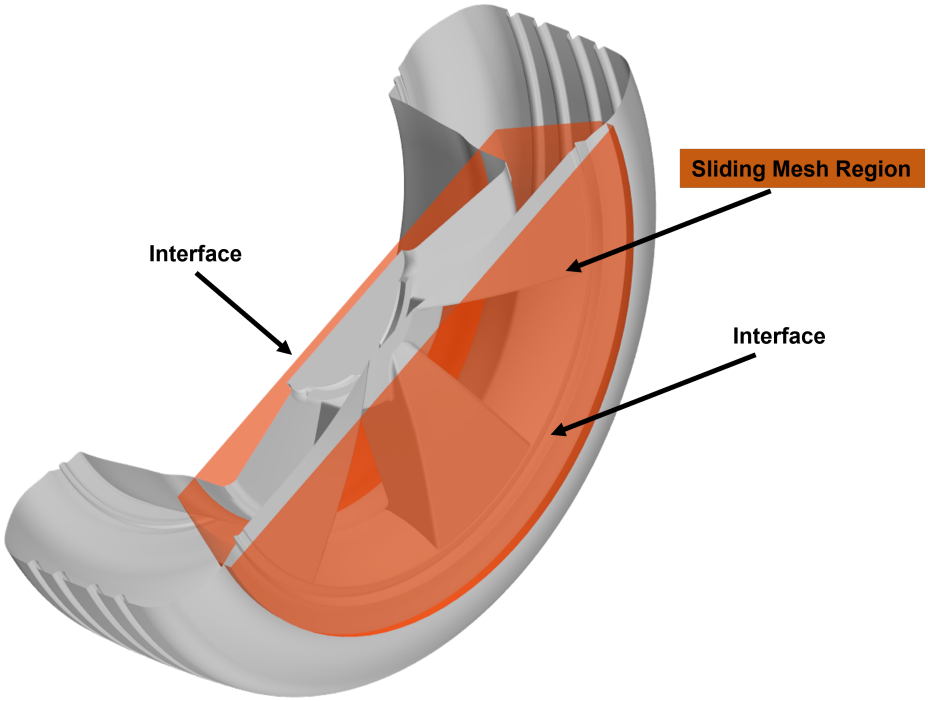


**Figure 3.6:** Cross-section of front-left wheel showing the sliding mesh region along with the interfaces

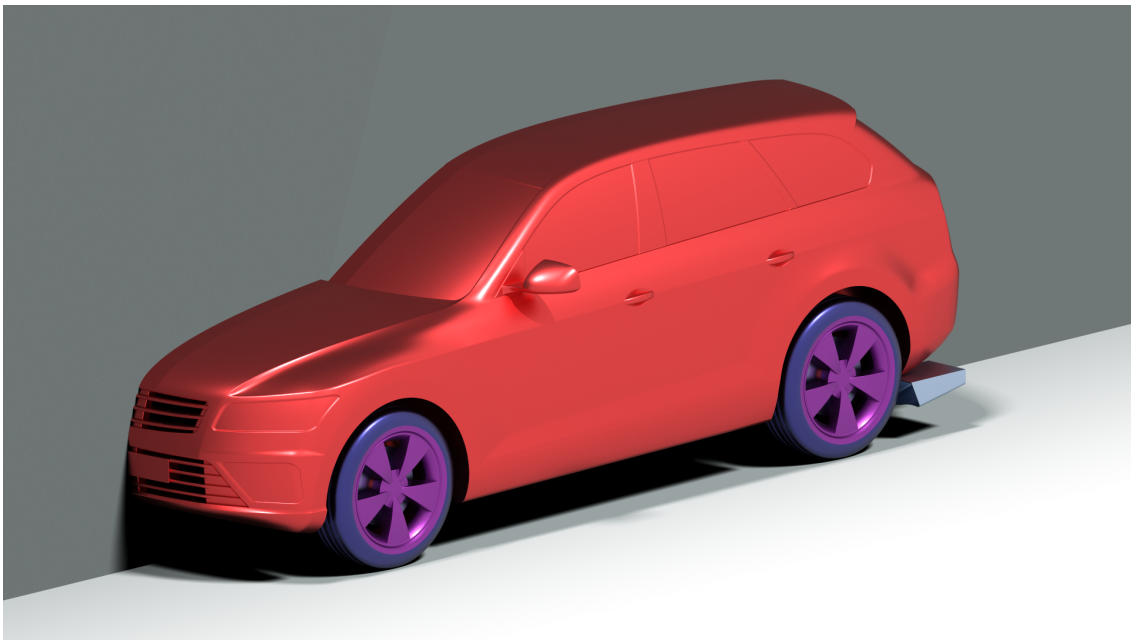

**Figure 3.7:** Magnified domain indicating the placement of vehicle and different boundary conditions depicted in various colours

### 3.2.3 Mesh

A polyhedral dominant mesh along with surface remesher and prism layers on all no-slip walls on the vehicle is used to mesh the entire domain. The cells are larger at the domain walls and they get finer close to the vehicle surface. This is done so to avoid having unnecessary refinements near the domain walls which are very far from the vehicle. Moreover, the point of interest is the flow behaviour close to the vehicle. By implementing large cells close to the domain walls, the total number of cells and the overall computational time and cost are reduced. The radiator at the front grille with a porous media region uses a hexahedral mesher to have directional flow as the flow inside the radiator is mostly unidirectional. The polyhedral meshers on the sliding mesh region are very fine (1mm cells) to capture finer details of the flow around wheels as shown in Figure 3.8.

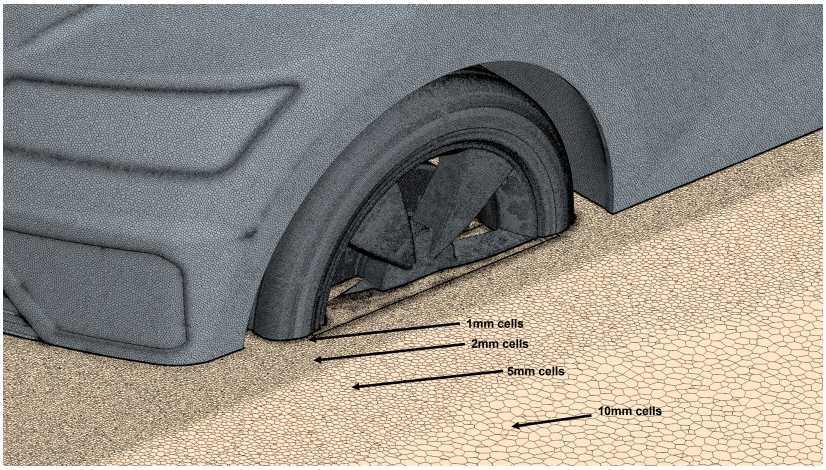


**Figure 3.8:** Mesh visualisations on z = 0 plane along with surface mesh

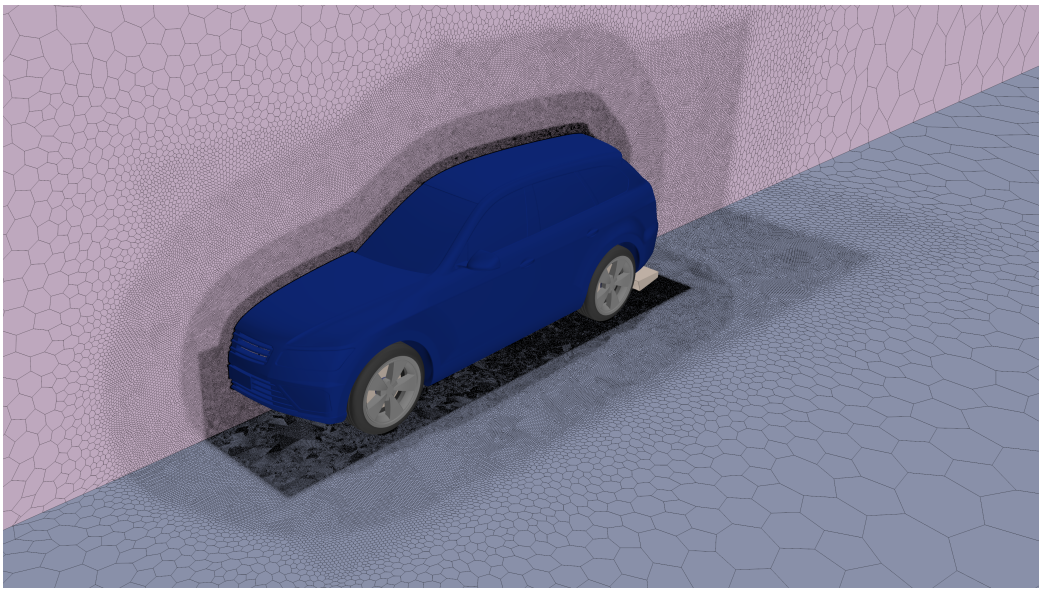

**Figure 3.9:** Mesh depicting the various volumetric refinements around the vehicle

Various mesh sizes and refinements were investigated to check grid dependency. From the baseline setup that consisted of 45 million cells, a finer setup with 67 million and 78 million cells were compared. The setup with 78 million cells shown in Figure 3.9 is used for all the transient simulations. The setup with a relatively coarser mesh consisting of 67 million cells were used for steady-state simulations.

Wall y+ indicates the non-dimensional cell height which helps determine if the mesh is coarse or fine. The finest mesh setup had low wall y+ range and finer refinements around the entire underbody of the vehicle. Prismatic layers on the vehicle surface along with volumetric refinements around the vehicle help in achieving an acceptable range of y+ for the $k\omega$ turbulence model as per StarCCM's recommendation. Most of the vehicle surface has a wall y+ of less than 1 but the entire vehicle lies within a wall y+ of 5 as shown in Figure 3.10.

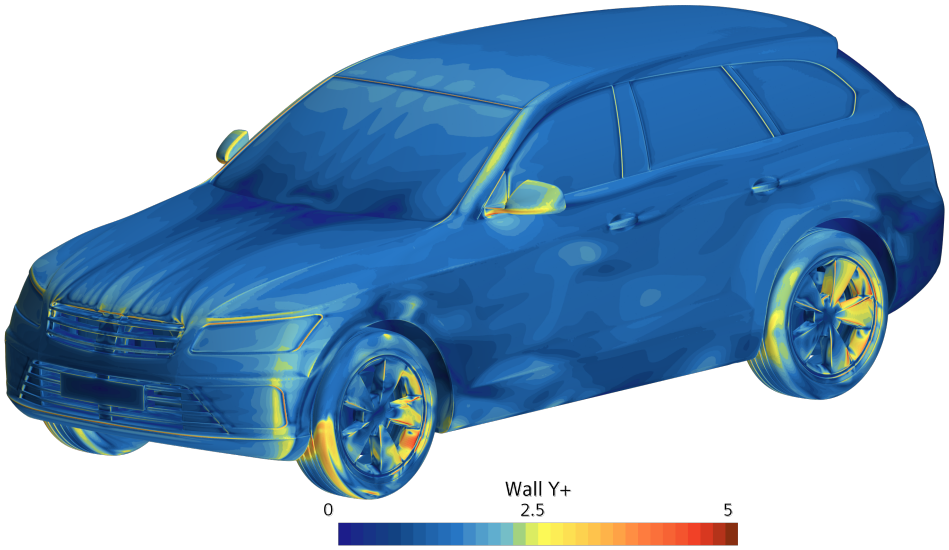


**Figure 3.10:** Wall y+ on the vehicle surface

### 3.2.4 Physics models

All of the simulations were performed using Reynolds Averaged Navier Stokes (RANS) approach. Initially, comparisons were made between k$\epsilon$ and SST-k$\omega$ physics models. Since the purpose of this work is to investigate the flow near walls whilst not compromising solutions in the free stream, SST-k$\omega$ proved to be a better option as it is a 2-equation eddy viscosity model. SST-k$\omega$ is a combination of both k$\epsilon$ and k$\omega$ which better predicts solution in the free stream and closer to the walls respectively.

Firstly, steady-state RANS simulations were conducted to compare the effects caused

by the addition of TTC's device onto the vehicle. Finally, transient RANS (URANS) simulations were conducted to implement sliding mesh for rim rotation. This allowed for investigation the complex flow behaviour around the wheels and closer to TTC's device. IDDES (Improved Delayed Detached-Eddy Simulation) physics model is now becoming an industrial standard to perform aerodynamic studies on vehicles. However, it was not implemented in this project due to its significantly higher computational cost and time.

### 3.2.5 Time step for transient runs

The transient simulations were started with a large time step of 1s which was allowed to run until the residuals stabilized. Next, the time-step is decreased by 1/10 $^{th}$ order of magnitude until reaching the lowest value of 5 $\times 10^{-4}$ s. The lowest time-step is 5 $\times 10^{-4}$ s because the results did not vary significantly for this mesh setup when the time-step is further reduced. The simulations were conducted until a physical time of 3.5 s with the lowest time step to stabilize the flow.

### 3.2.6 Section planes to interpret results

Figure 3.11 shows the different section planes used to illustrate results. The section planes are as follows:

- Centreline plane (y = 0): Longitudinal section plane through the centre of the vehicle.
- Section plane (z = 0): Horizontal plane at z = 0 passing through the wheel centre.
- Section plane 1: Longitudinal section plane passing through the centre of TTC's device.
- Section plane 2: Lateral section plane passing through TTC's device

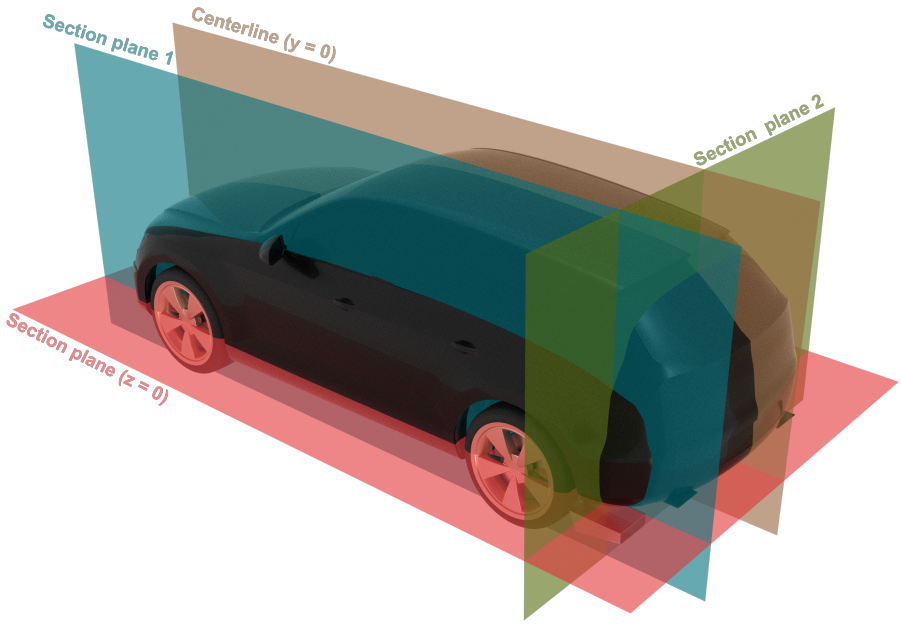


**Figure 3.11:** Various section planes used to illustrate the results

# 4

# Results

## 4.1 Comparison study with and without TTC's device using steady-state RANS simulations

### 4.1.1 Pressure coefficient

Figure 4.1 below shows the differences in contours of pressure coefficient on the rear-end of the vehicle. The position of base pressure region appears slightly higher with the implementation of the device. This is due to additional upwash generated because of the shape of the device. On the other hand, a low-pressure area is seen on the rear wheels indicating accelerated flow which may be caused due to the restricted area behind the rear wheels.

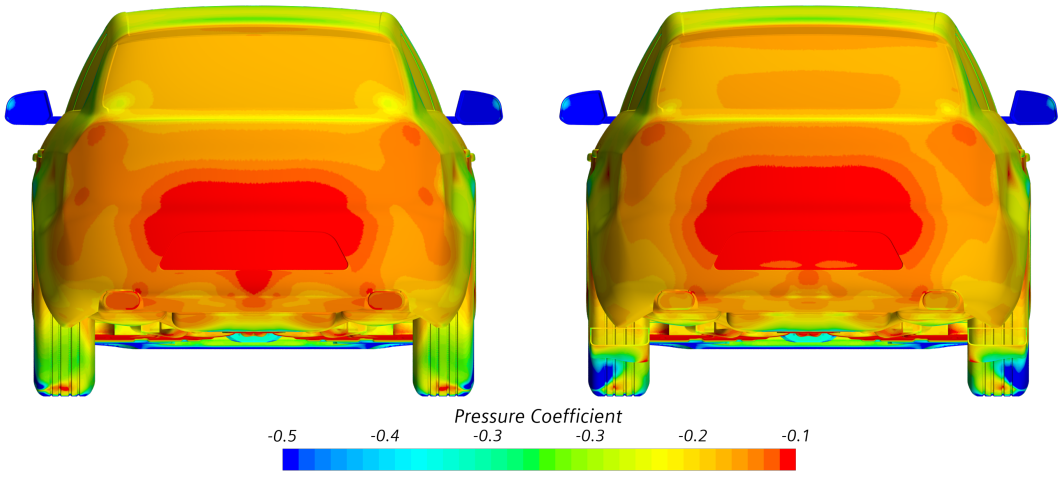


**Figure 4.1:** Comparison of pressure coefficients without the device (left) and with the device (right) on rear-end of the vehicle

### 4.1.2 Isosurfaces of total pressure

Figure 4.2 below shows the differences in isosurfaces of total pressure on the vehicle. Variations in the magnitude of the rear wake are noted. The upwash and downwash vary by a few degrees. The overall magnitude of the rear wake profile is slightly larger in the case of the vehicle with the device.

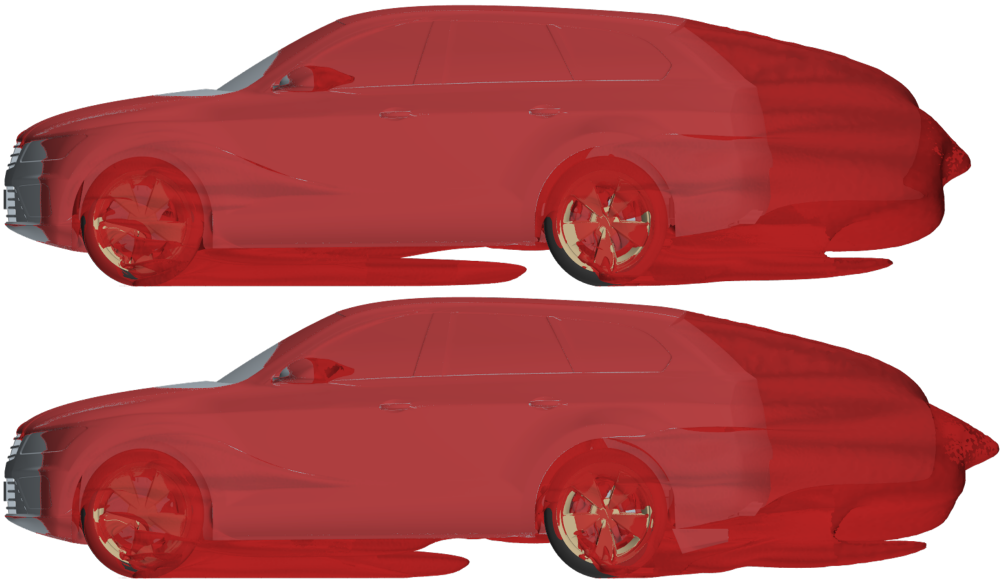

**Figure 4.2:** Comparison of isosurfaces of total pressure without the device (top) and with the device (bottom)

### 4.1.3 Drag and lift coefficients

Figure 4.3 indicates the $C_d$ values with respect to physical time. For all the transient simulations, the results were averaged for a physical time of approximately 1.6s to obtain the drag and lift coefficients.

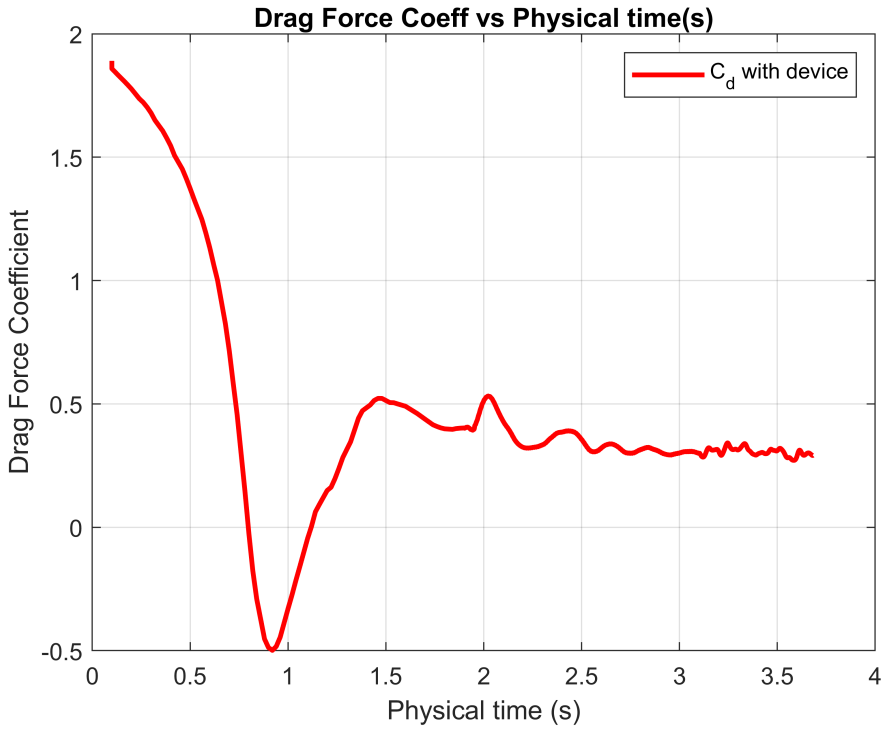


**Figure 4.3:** Coefficient of drag plot from a transient simulation

**Table 4.1:** Drag coefficients ($C_d$) and lift coefficients ($C_{lf}$, $C_{lr}$) obtained from CFD simulations

| | | $C_d$ | $C_{lf}$ | $C_{lr}$ |
|---|---|---|---|---|
| Reference (CFD)* | | 0.328 | -0.009 | -0.014 |
| $k\omega$ RANS | without device | 0.287 | -0.006 | -0.011 |
| | with device | 0.291 | -0.007 | -0.012 |
| $k\omega$ URANS | without device | 0.326 | -0.007 | -0.013 |
| | with device | 0.331 | -0.008 | -0.017 |

To validate the change in the rear wake, drag coefficients were investigated. Table 4.1 shows the $C_d$, $C_{lf}$ and $C_{lr}$ values for both with and without TTC's device for steady-state and transient RANS simulations. The reference value for $C_d$ of 0.328 for the AeroSUV is obtained from a previous study [14]. When the device is included, the drag coefficient of the vehicle increases by 4 and 5 drag counts (1 drag count = 0.001 $C_d$) for steady-state and transient RANS respectively. The relative differences in $C_d$ between the reference value and the values obtained in this analysis might be due to various factors such as mesh quality, physics models used, variations in cooling drag, etc. Furthermore, it is noted from the obtained results that all the cases produce downforce on the rear axles (i.e., negative lift force on rear axle).

### 4.1.4 Velocity magnitude

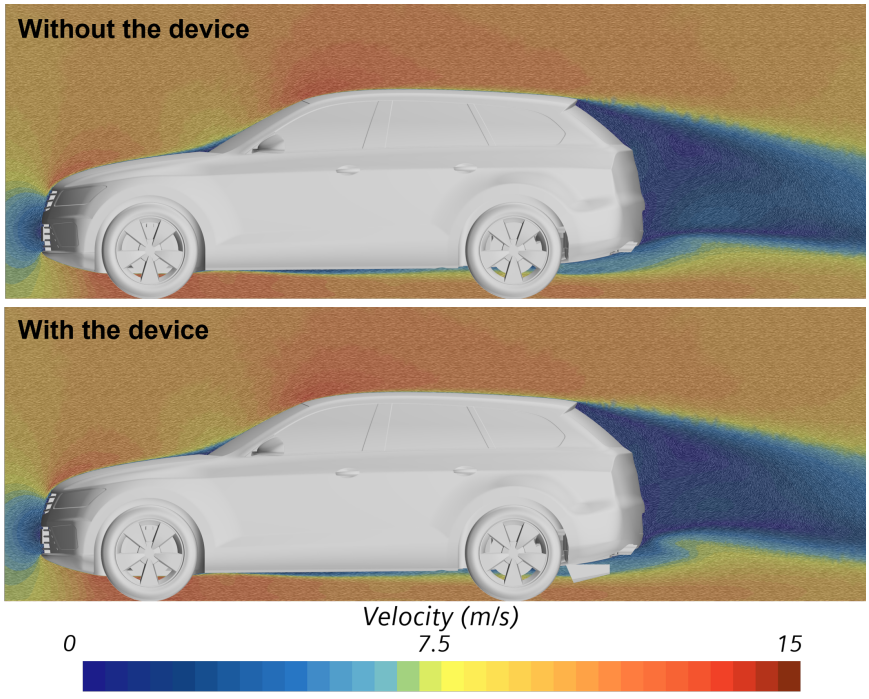


**Figure 4.4:** Comparison of velocity magnitude on centreline plane(y=0) without the device (top) and with the device (bottom)

Figure 4.4 shows the comparisons of velocity magnitudes on the centreline plane i.e., y = 0. The main influence of the addition of TTC's device is the change in upwash. Since the device is placed behind both rear wheels, the change in flow structures behind the wheels is seen to influence the velocity profile on the centreline plane. To validate the influence of the device, velocity magnitudes on a section plane through the device as shown in Figure 4.5 are considered. This clearly indicates accelerated flow underneath the device due to the restricted flow behind the wheels relative to just having the actual vehicle. On the other hand, flow recirculation is seen at the inlet of the device.

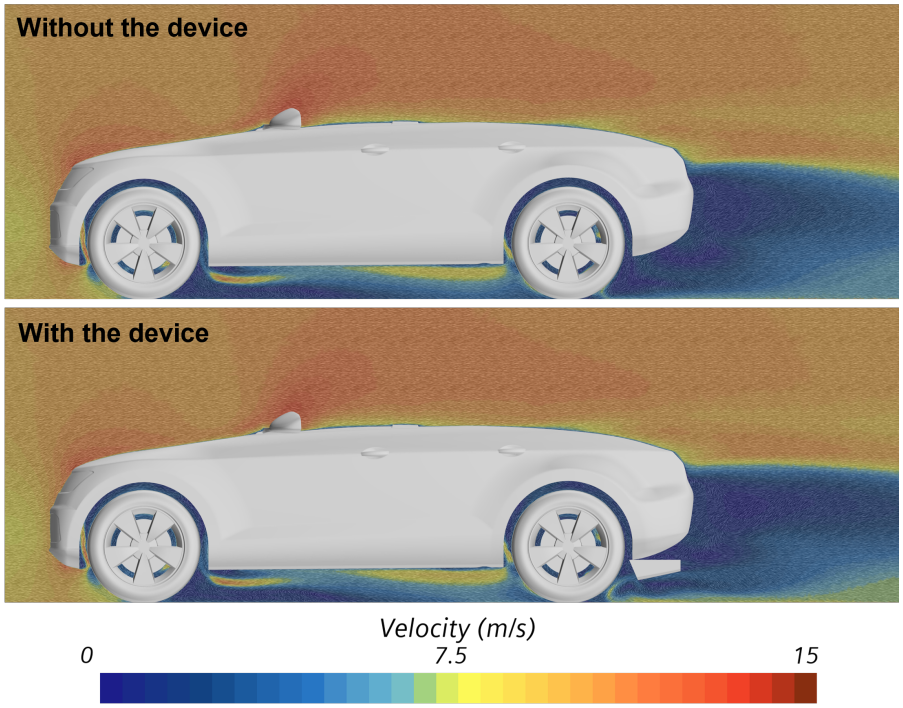


**Figure 4.5:** Comparison of velocity magnitude on section plane 1 without the device (top) and with the device (bottom)

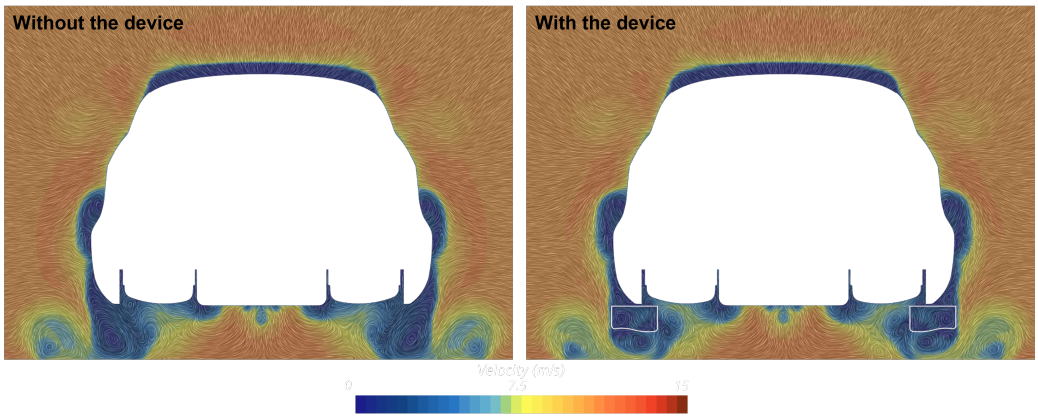


**Figure 4.6:** Comparison of velocity magnitude on section plane 2 without the device (left) and with the device (right)

Figure 4.6 shows the frontal view comparisons of velocity magnitudes on the section plane through the device. It is seen that the device generates additional smaller vortices both inside and on the walls of the device. These vortices seem to be formed due to the inlet shape and a converging side profile. The walls of the device act as blades with an angle of attack. In this study, the forces on the axles were not investigated. However, it can be seen that the device modifies the downforce at the rear which is also shown by $C_{lr}$ values on Table 4.1.

## 4.2 Comparison study between RANS and URANS with TTC's device

### 4.2.1 Pressure coefficient

Figure 4.7 shows the differences in contours of pressure coefficient on the rear-end of the vehicle between steady-state and transient RANS simulations. The magnitude of base pressure region significantly changes in transient RANS. This is due to the implementation of sliding mesh i.e., physical rotation of the mesh with every time-step. Slight variations on the pressure behind rear wheels are observed. Transient simulations allow to capture a more detailed flow behaviour relative to steady-state.

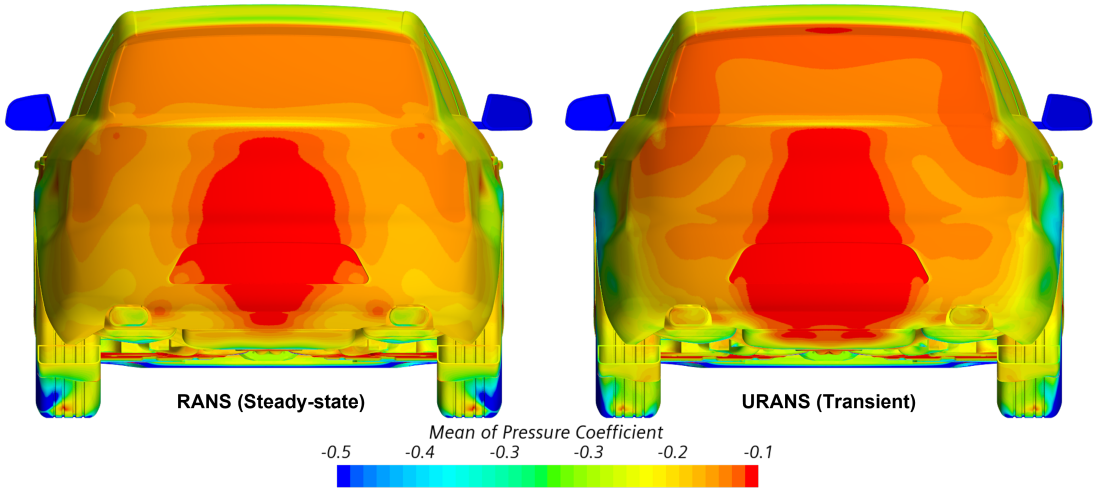


**Figure 4.7:** Comparison of time averaged pressure coefficient: steady-state RANS (left) and transient RANS (right)

### 4.2.2 Velocity magnitude

Figure 4.8 shows the comparisons of velocity magnitudes on the centreline plane i.e., y = 0 and a section plane passing through the device. With URANS, the rear wake profile behind the vehicle changes drastically. The flow acceleration under the vehicle is captured in more detail in transient RANS. Boundary layer formations on the sides of the vehicle are only observed in transient RANS.

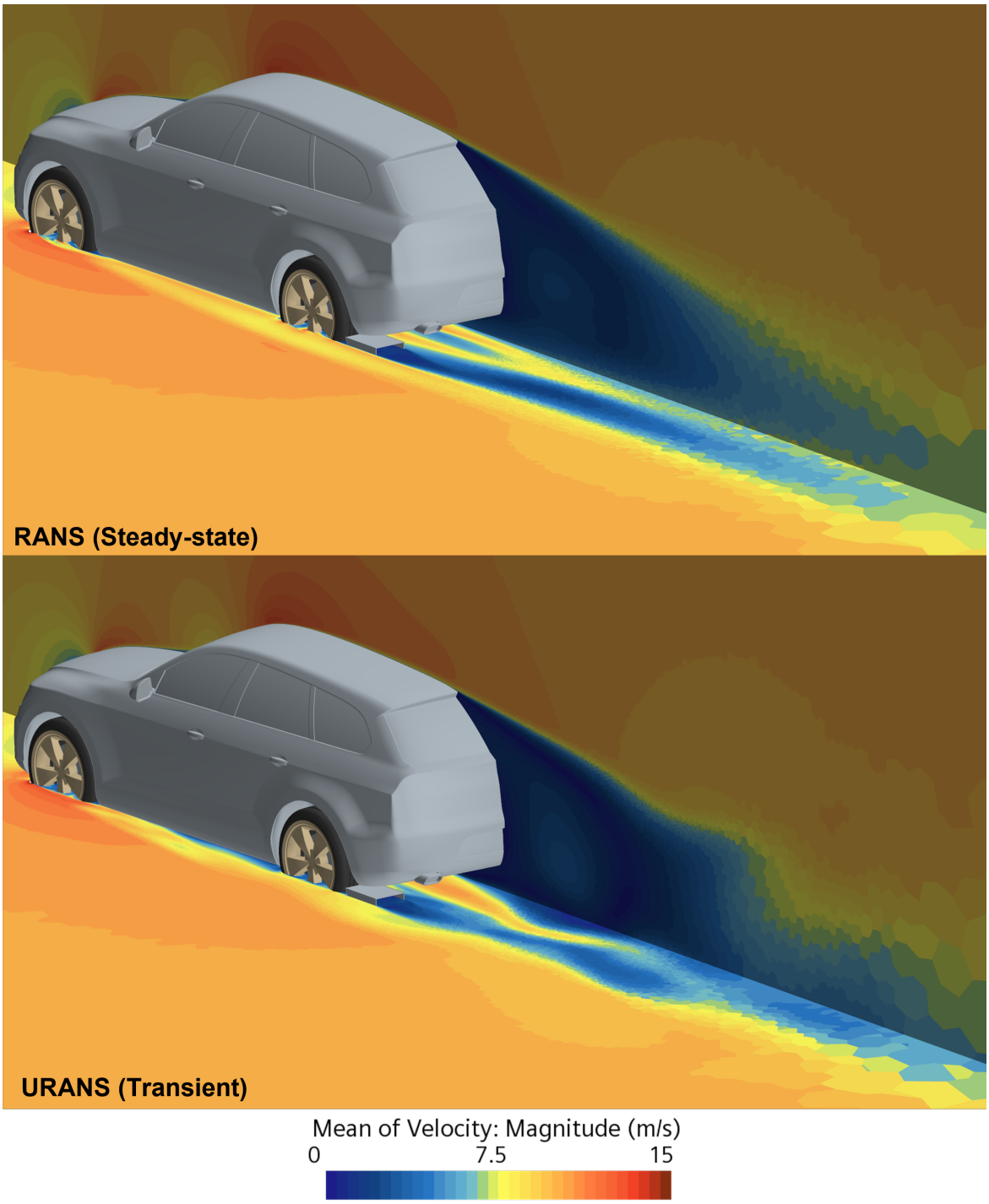


**Figure 4.8:** Comparison of time averaged velocity magnitude: steady-state RANS (left) and transient RANS (right)

## 4.3 Transient RANS with TTC's device

### 4.3.1 Isosurfaces of total pressure

Figure 4.9 indicates the isosurfaces of time averaged total pressure which shows the complex wake structures generated around the wheels and close to the device. A previous study with a much more sophisticated numeric setup also showcased the complex velocity field behind rotating wheels. It also indicated vortices generated at the wheel shoulder, contact patch, inner/outer tyre contact, etc [26].

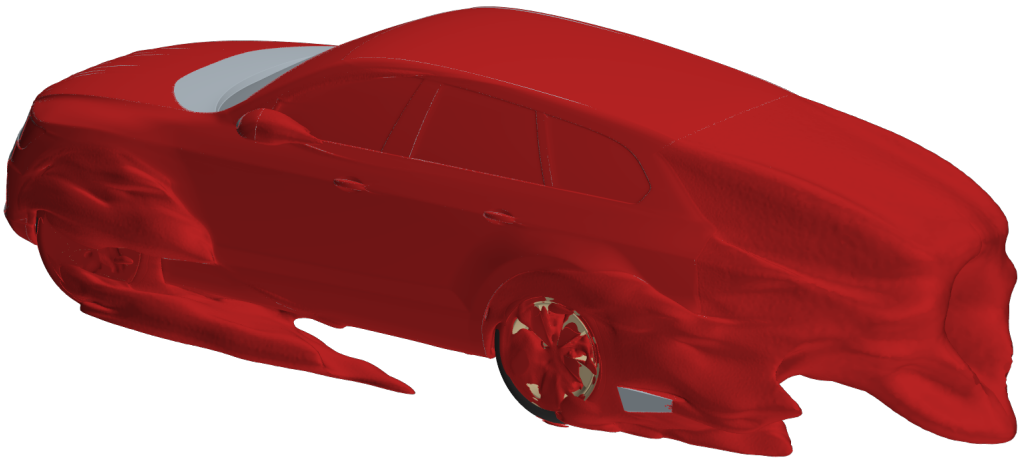

**Figure 4.9:** Isosurfaces of time averaged total pressure for URANS

### 4.3.2 Streamlines

Streamline tracers were used to determine the flow entering the device. Figure 4.10 shows streamlines with multiple seed points inside the device which are traced both ways. To elaborate, the streamlines show where the flow comes from and also where it goes. This allows for visualization the air flow through the device. Figure 4.11 shows different views of these streamlines indicating the flow downstream that wraps around the rear wheels before entering the device. Figures 4.11a and 4.11c show the rear and underbody views respectively. Another flow behaviour that is noted here is that a higher magnitude of flow through the device is from the underbody or inner side of the tyres.

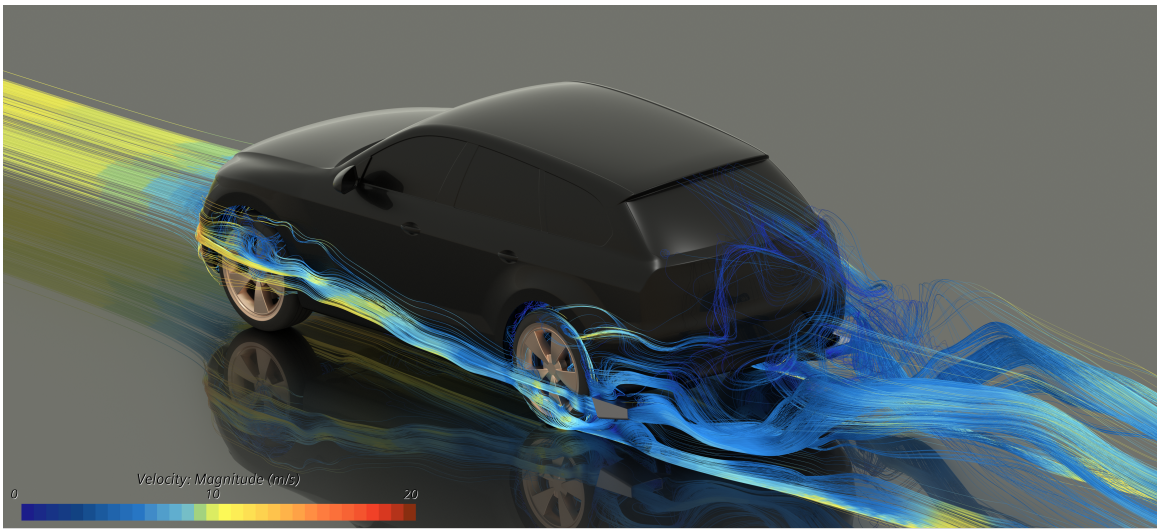


**Figure 4.10:** Streamlines originating within TTC's device traced both ways

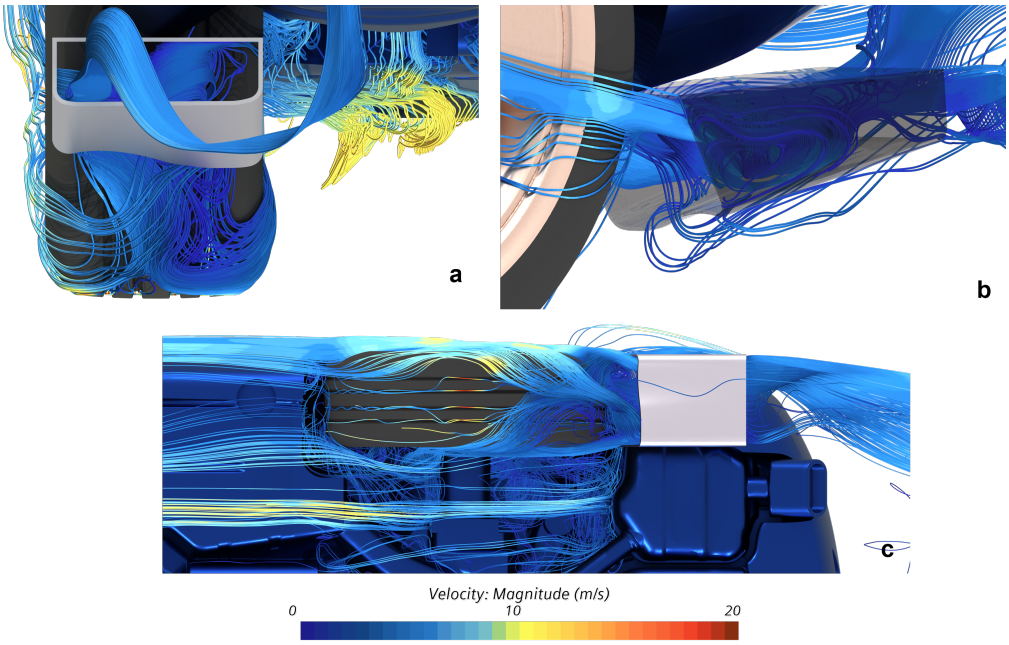


**Figure 4.11:** Streamline views indicating flow around the rear wheels

Figure 4.11 b emphasizes the flow recirculation occurring at the inlet. The bottom portion of the device due to its shape and angle of attack causes flow separation at the edges. The shape also generates vortices which tend to carry particles moving with the flow away from the inlet. This recirculation phenomenon is represented using tracers as shown in Figure 4.12 on the streamlines that simulate superficial particles that move with the flow stream. It is noted that only 20% of the introduced particles at the tyre patch of the rear wheels entered the device. Furthermore, the mass flow of air through the device is reduced to 15% when placed behind the rear wheels relative to having just the device in an open domain. It is indicative that the mass flow of air decreases by approximately 80% to 85%.

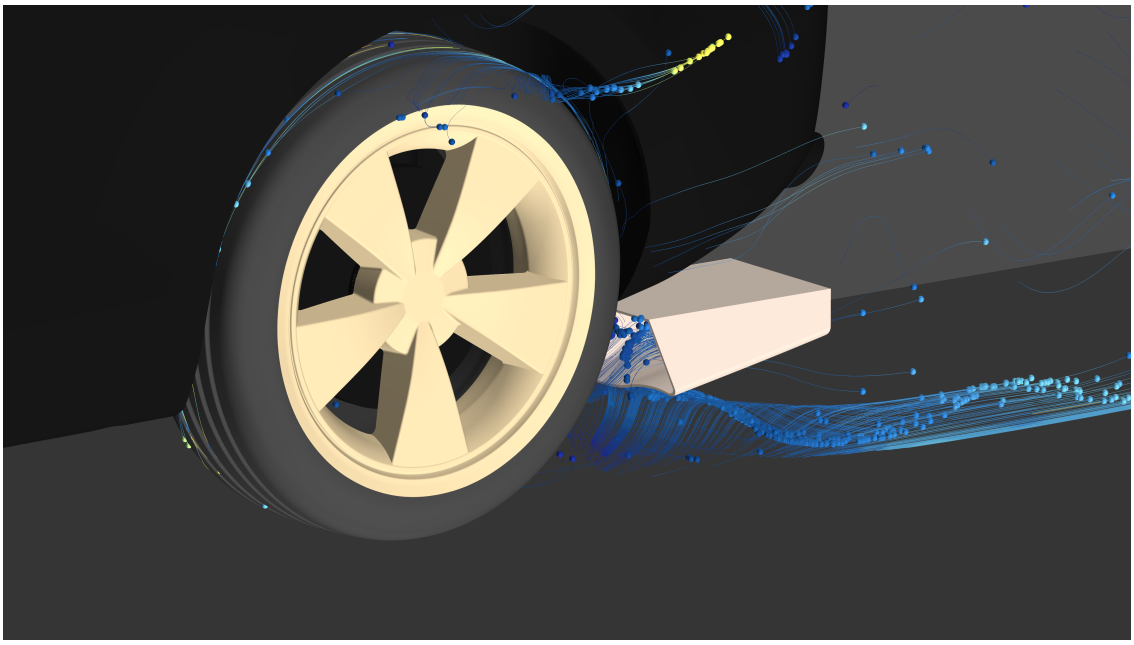

**Figure 4.12:** Superficial particles originating from the tyre patch

## 4.4 Design proposals

Based on the analysis, an externally mounted collector device is not ideal. Several vehicle attributes such as external aerodynamics, aeroacoustics, contamination, energy management and thermal efficiency, affect the method of PM collection. The Figure 4.13 and 4.15 proposes a few design choices that could yield better PM collection rates.

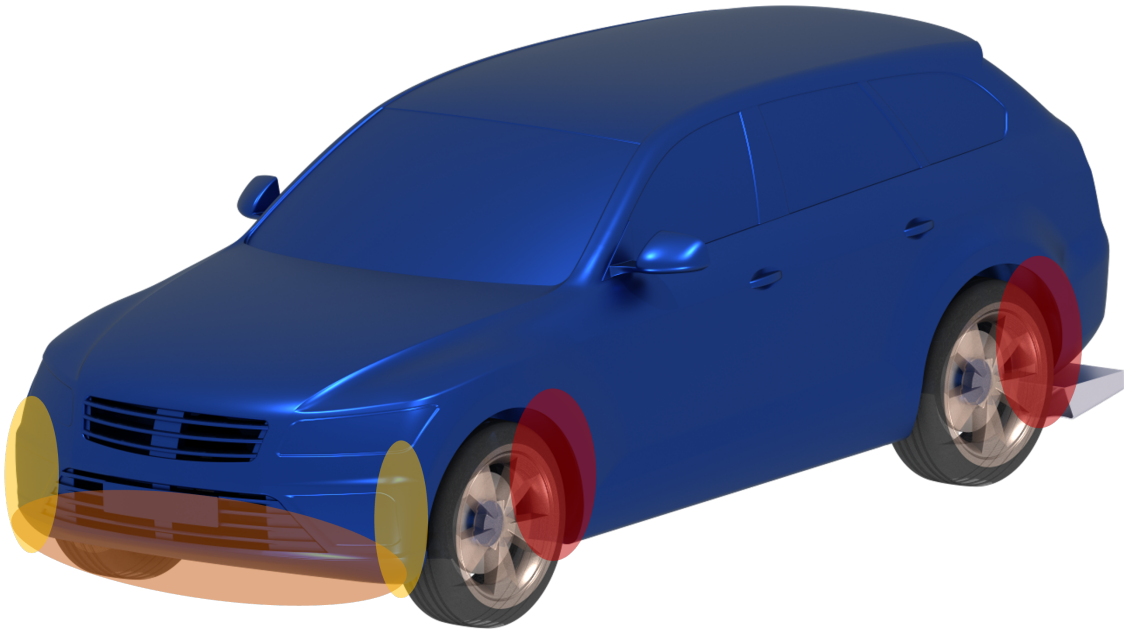

**Figure 4.13:** Design proposal 1

In Figure 4.13, internally mounted array of electrostatic plates within the wheel-house is indicated in "red". To direct more flow through this area, a modification to the frontal area is made to introduce air-curtains as shown in Figure 4.14 [27] which is indicated in "yellow". The air-curtains also help in reducing drag on the vehicle caused due to wheel rotation. However, the angle of attack on the intake can be optimised such that the "laminar" flow stream is directed at the electrostatic plates inside the wheel-house. Finally, a much larger device is placed within the front grilles of the BEV indicated in "orange". This allows for TWP emitted from the vehicle in front as well as road dust that are suspended above the road surface.


**Figure 4.14:** Indication of laminar flow created by air-curtains [27]

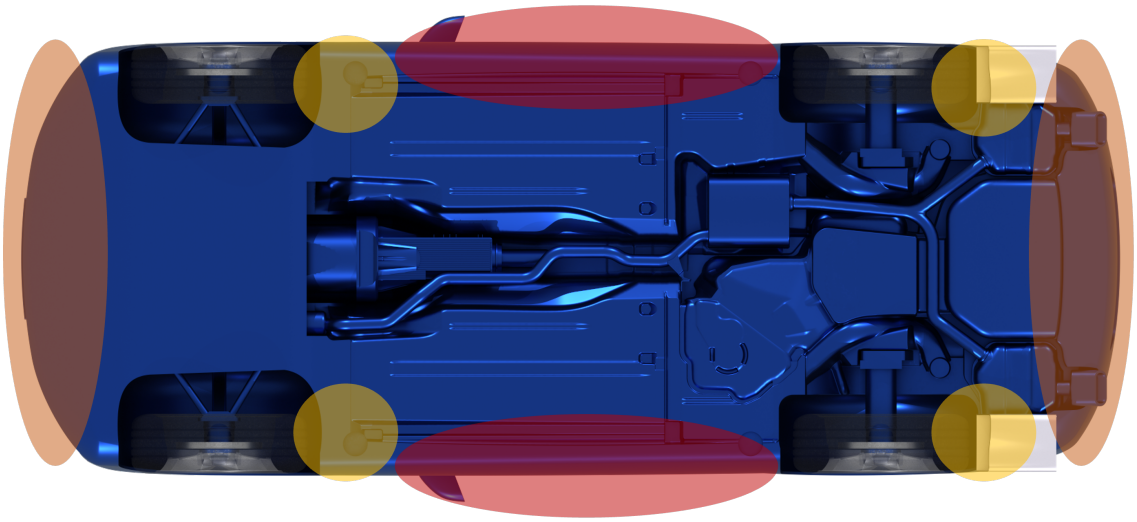

**Figure 4.15:** Design proposal 2

Figure 4.15 shows suction fans mounted behind each wheel indicated in "yellow". These fans help to generate suction force behind each wheel that helps pull the TWPs into the vehicle body. To be more energy efficient, NACA ducts can be implemented to generate inward flow or suction. The regions indicated in "red" shows the array of electrostatic plates that are placed along the sides of the vehicle. This helps capture PM from the front wheels. For capturing PM emitted at the rear wheels, a large device is mounted both at the rear and the front indicated in "orange".

Moreover, from Figure 4.11a it is seen that majority of the flow is concentrated towards one side of the device. Hence utilizing the device partially. To help direct or guide the flow towards the locations where the bulk of the flow stream is not concentrated, guide vanes can be implemented under the body. Also, vortex generators can help direct the flow to a desired location.

The implementation of these design features can be varied based on many factors but mostly energy efficiency and available packaging space on the vehicle. Also to note, are that some of these features on the vehicle such as air-curtains, vortex generators or NACA ducts will only work effectively when the vehicle is moving above a certain threshold velocity. Once the TWPs are stuck to the electrostatic plates, the charge on the plates can be reversed frequently to repel the PM from the plates. These PM are ideally collected in a tank placed under each electrostatic plate array.

# 5
# Conclusion

Throughout this thesis work, the main aim has been to investigate the air flow around rotating wheels in a passenger vehicle using numerical simulations. Thus, determining the motion of airborne tyre PM that originates at the tyre patch. Additionally, the inclusion of the collector device from The Tyre Collective allowed for further investigations of efficiently capturing these PM and the complexities of having an externally mounted device.

Investigations of steady-state comparisons of the influence of TTC's device showed that by including the device behind the rear wheels, the shape of rear wake slightly changes. Moreover, there is more upwash generated that moves the rear base pressure region slightly higher relative to having just the vehicle in the domain. TTC's device also restricts flow behind the rear wheels to some extent, causing flow accelerations under the device. On the other hand, transient simulations depicted flow re-circulations at the inlet of the device. The streamline tracers or superficial particles which were introduced at the tyre patch helped visualize the flow recirculations. It also indicated that only 20% of the introduced streamline tracers entered the device as shown in Figure 4.12. Moreover, comparing mass flow of air through the device in an open domain relative to mounting it behind the rear wheels showed that the mass flow reduced to 15%. This clearly indicates that to capture more airborne PM emitted from tyres, there must be more air flow pushed through the device at any given time.

## 5.1 Future work

This study along with an elaborate literature review and the upcoming governmental regulations show that tyre wear particulate matter will be regulated in the near future. Vehicle manufacturers must comply to these stringent regulations. The thesis work establishes a base to start developing effective solutions and the knowledge required to numerically simulate these particles. Targeted at increasing the understanding of these non-exhaust emissions, several experimental and numerical studies are proposed. Furthermore, a generic vehicle model is used in this work. However, production vehicle geometries with active and passive aerodynamic features can be considered in further research.

### 5.1.1 Experimental work

- Setup a rig with controlled tyre temperature to study and understand temperature effects

- Mount existing / improvised collection device at various locations on a vehicle to compare on-road collection rates
- Experiment with different orientations of the electrostatic plates on the existing device
- Experiment with different mounting angles of the existing device

### 5.1.2 Numerical work

- Validate some of the experimental suggestions using numerical simulations to isolate promising solutions
- Develop a methodology to simulate tyre particle emissions with better physics (ID-DES and multiphase simulations)
- Study the effects of various driving conditions mainly crosswinds and driving cycles
- Validate based on the experimental work, regions to optimally capture these particles with a rate of collection over 50% of the emitted PM

# Bibliography


[1] B. Bilgin et al., 2015, "Making the Case for Electrified Transportation", in IEEE Transactions on Transportation Electrification, June, vol. 1, no. 1, pp.4-17.

[2] OECD, 2020, "Non-exhaust Particulate Emissions from Road Transport: An Ignored Environmental Policy Challenge", OECD Publishing, Paris.

[3] Kim, Gibaek; Lee, Seokhwan, 2018, "Characteristics of Tire Wear Particles Generated by a Tire Simulator under Various Driving Conditions", In Environmental science and technology 52 (21), pp.12153–12161.

[4] https://www.youtube.com/watch?v=ybZLjE_Xu6M [Accessed on 2022-03-11]

[5] Juanita Rausch, David Jaramillo-Vogel, Sébastien Perseguers, Nicolas Schnidrig, Bernard Grobéty, Phattadon Yajan, 2022, "Automated identification and quantification of tire wear particles (TWP) in airborne dust: SEM/EDX single particle analysis coupled to a machine learning classifier", Science of The Total Environment, Volume 803, 149832, ISSN 0048-9697.

[6] Stephan Wagner, Philipp Klöckner, Thorsten Reemtsma, 2022, "Aging of tire and road wear particles in terrestrial and freshwater environments – A review on processes, testing, analysis and impact", Chemosphere, Volume 288, Part 2, 132467, ISSN 0045-6535.

[7] P. Sundt, R. S, T.R. Haugedal, P.-E. Schulze, 2021, "Norske landbaserte kilder til mikroplast (Norwegian Land-based Sources to Microplastics)", MEPEX, Oslo, p. 88

[8] https://www.emissionsanalytics.com/news/gaining-traction-losing-tread [Accessed on 2022-06-17]

[9] Zhengyu Men, Xinfeng Zhang, Jianfei Peng, JingZhang, Tiange Fang, Quanyou Guo, Ning Wei, Qijun Zhang, Ting Wang, LinWu and Hongjun Mao, 2022, "Determining factors and parameterization of brake wear particle emission", Journal of Hazardous Materials.

[10] https://www.thetyrecollective.com [Accessed on 2022-05-24]

[11] Vanherle, K., Lopez-Aparicio, S., Grythe, H., Lükewille, A., Unterstaller, A., and Mayeres, I., 2021, "Transport Non-exhaust PM-emissions: An overview of emission estimates, relevance, trends and policies".

[12] Fackrell, J. E., and J. K. Harvey. 1973. The flow field and pressure distribution of an isolated road wheel. Stephens, H.S., Ed. Advances in Road Vehicle Aerodynamics. 1973. BHRA Fluid Engineering, Cranfield, 1973, P. 155-165.

[13] https://www.ecara.org/reference-models [Accessed on 2022-01-23]

[14] Zhang, C., Tanneberger, M., Kuthada, T., Wittmeier, F. et al., 2019, "Introduction of the AeroSUV-A New Generic SUV Model for Aerodynamic Research", SAE Technical Paper 2019-01-0646.

[15] Tomasz Gonet, Barbara A. Maher, Ilona Nyirő-Kósa, Mihály Pósfai, Miroslav Vaculík, Jana Kukutschová, 2021, "Size-resolved, quantitative evaluation of the magnetic mineralogy of airborne brake-wear particulate emissions", Environmental Pollution, Volume 288, 117808, ISSN 0269-7491.

[16] Karagulian, F.; Belis, C. A.; Dora, C. F. C.; Pruss-Ustun, A. M.; Bonjour, S.; Adair-Rohani, H.; Amann, M., 2015, "Contributions to cities' ambient particulate matter (PM): A systematic review of local source contributions at global level",. Atmos. Environ., 120 (Supplement C), pp.475-483.

[17] Timmers,V. and P. Achten, 2016, "Non-exhaust PM emissions from electric vehicles", Atmospheric Environment, Volume 134, pp.10-17.

[18] Martin Rexeis, Stefan Hausberger, 2009, "Trend of vehicle emission levels until 2020 – Prognosis based on current vehicle measurements and future emission legislation", Atmospheric Environment, Volume 43, Issue 31, pp.4689-4698.

[19] Adachi, K., Tainosho, Y., 2004, "Characterization of Heavy Metal Particles Embedded in Tire Dust", Environment international, 30(8), 1009-17.

[20] Teddy Hobeika, 2018, "Wheel Modelling and Cooling Flow Effects on Car Aerodynamics", ISBN 978-91-7597-687-7.

[21] Marisa L. Kreider, Julie M. Panko, Britt L. McAtee, Leonard I. Sweet, Brent L. Finley, 2010, "Physical and chemical characterization of tire-related particles: Comparison of particles generated using different methodologies", Science of The Total Environment, Volume 408, Issue 3, pp.652-659.

[22] https://uk-air.defra.gov.uk/, 2019, "Non Exhaust Emissions typeset Final". [Accessed on 2022-05-16]

[23] Pehlken, Alexandra and Essadiqi, E., 2005, Scrap Tire Recycling in Canada.

[24] Maurizio Gualtieri, Laura Rigamonti, Valentina Galeotti, Marina Camatini, 2005, "Toxicity of tire debris extracts on human lung cell line A549", Toxicology in Vitro, Volume 19, Issue 7, pp.1001-1008.

[25] Mats Gustafsson, Göran Blomqvist, Anders Gudmundsson, Andreas Dahl, Erik Swietlicki, Mats Bohgard, John Lindbom, Anders Ljungman, 2008, "Properties and toxicological effects of particles from the interaction between tyres, road pavement and winter traction material", Science of The Total Environment, Volume 393, Issues 2–3, pp.226-240.

[26] Wäschle, A., 2007, "The Influence of Rotating Wheels on Vehicle Aerodynamics - Numerical and Experimental Investigations", SAE Technical Paper 2007-01-0107.

[27] BMW Efficient Dynamics - BMW Air Curtain Technology (11/2012), https://www.press.bmwgroup.com/global/photo/detail/P90107377/bmw-efficientdynamics-bmw-air-curtain-technology-11-2012 [Accessed on 2022-05-12]

**DEPARTMENT OF MECHANICS AND MARITIME SCIENCES**
**CHALMERS UNIVERSITY OF TECHNOLOGY**
Gothenburg, Sweden
www.chalmers.se


CHALMERS
UNIVERSITY OF TECHNOLOGY